Measurements Within Vortex Cores in a Turbulent Jet

Amit Agrawal
e-mail: agrawaa@me.udel.edu

Ajay K. Prasad
e-mail: prasad@me.udel.edu

Department of Mechanical Engineering,
University of Delaware,
Newark, DE 19716

High-pass filtering of instantaneous two-dimensional PIV data is employed to educe vortices occurring in the axial plane of a self-similar turbulent axisymmetric jet. An automated method is used to identify the vortices and to measure circulation, tangential velocity, vorticity, and centrifugal force within their cores (defined here as the region within the largest closed streamline). Results include radial variation of these quantities within vortex cores, and the energy of vortices. We find that the vorticity is maximum at the vortex center and decreases monotonically with the radial coordinate. Results indicate that the center of a larger vortex spins faster than a smaller vortex (in an ensemble averaged sense); however, the trend reverses to give the expected result at the core edge. Vorticity results for different vortex radii collapse upon normalization. The average energy of vortices is seen to increase as the square of the vortex radius. In addition, three possible regimes of vortex number versus vortex size are suggested by our data.
[DOI: 10.1115/1.1568357]

Introduction

Turbulent flows are characterized by vortices ranging in size from the integral length scale down to the Kolmogorov scale. The two ends of the range of vortex scales are associated with different properties. For example, large-scale vortices account for most of the turbulent energy, while the small scales carry almost the entire vorticity. Even for a given vortex size, the range of their associated properties is expected to be large. These notions have proved extremely useful in understanding the nature of turbulence. In this paper, we provide direct measurement of vortex properties to substantiate these ideas.

To date, researchers have found it rather difficult to educe instantaneous structures from turbulence data. By their very nature, pointwise techniques lack spatial resolution which is imperative for visualizing and measuring the properties of these structures; at best, pointwise techniques must rely on conditional averaging to expose only the dominant structures. Consequently, experimental data about properties of vortical structures in different flow fields is rather scarce, and especially the nature of the vortex core is virtually unexplored.

PIV can provide velocity information with substantially greater spatial resolution. Further, high-pass filtering can be employed to educe vortical structures from instantaneous two-dimensional PIV frames (Adrian et al. [1], and Agrawal and Prasad [2]). Agrawal and Prasad [2] applied high-pass filtering to PIV data of a turbulent jet, and presented statistical distributions of vortex radius, circulation, vorticity, and energy as a function of Reynolds number and radial position. In [3], we applied low-pass filtering to examine the various organizational modes of large vortices in a turbulent jet. In this paper, we use the same high-pass filtering technique to focus on the detailed properties *within* vortex cores.

Three types of vortex cores are commonly described in the literature—potential, Rankine and Lamb. A potential vortex possesses a $1/r$ tangential velocity (v_θ) distribution within its core; however, due to a singularity at the origin, it clearly cannot exist in nature. The singularity is removed in a Rankine vortex which has a core with a solid-body like rotation (constant angular velocity), while the flow outside the core is irrotational. Therefore, $v_\theta \sim r$ inside the core, and $v_\theta \sim 1/r$ beyond it (Fig. 1, adapted from Kundu [4]). It should be noted that for a real vortex, the presence of viscosity will smooth out the abrupt change in slope of v_θ at the core edge. For Lamb vortices vorticity within the core decays exponentially with the radial coordinate. Both Rankine and Lamb vortices are expected to better resemble a real vortex. However, Rankine vortices are somewhat easier to model, and so we will compare and contrast our results with them wherever appropriate.

Some theoretical studies of viscous vortex cores have been conducted in the past. For example, Mayer and Powell [5] derived the distribution of angular, axial, and radial velocities for a viscous core starting from the Navier-Stokes equations. They assumed the flow quantities to be self-similar within the core, and that the

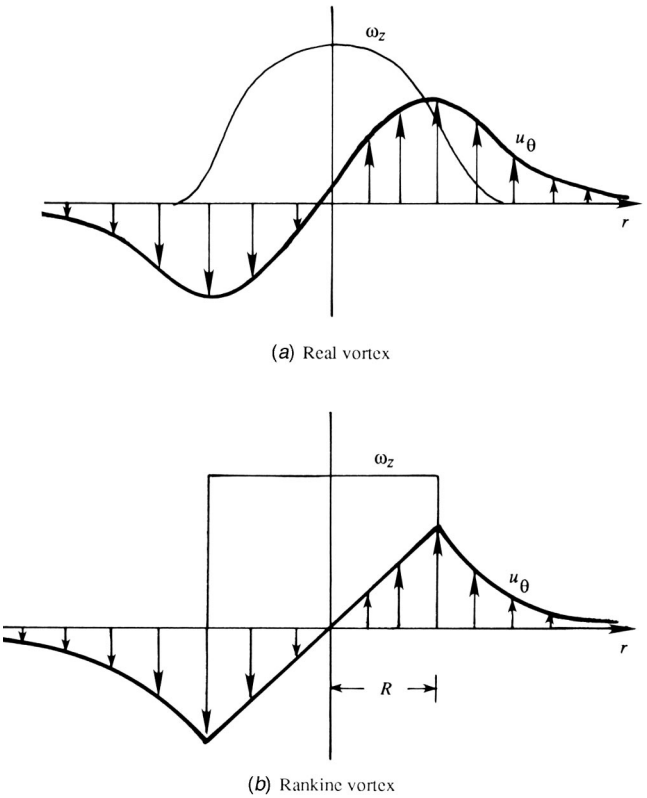

Fig. 1 Velocity and vorticity distributions in (*a*) a real and (*b*) a Rankine vortex (adapted from Kundu [4])

Contributed by the Fluids Engineering Division for publication in the JOURNAL OF FLUIDS ENGINEERING. Manuscript received by the Fluids Engineering Division March 13, 2002; revised manuscript received September 15, 2002. Associate Editor: M. Plesniak.

carrier fluid had a simple algebraic velocity distribution. From their angular velocity result they report a solid-body rotation near the vortex axis, and an inviscid solution outside the core. On the experimental side, measurements have been made for a tip vortex of an airfoil, and vortex rings. For example, Desabrais and Johari [6] used an ultrasound method to measure the circulation of a tip vortex, and found that the circulation is maximized when the entire vortex core is enclosed within the measurement path. Maxworthy [7] obtained LDA measurements inside the cores of laminar and turbulent vortex rings and found that the change from a constant ω to radially varying ω is much sharper for turbulent vortex rings.

The situation for Mayer and Powell [5], Desabrais and Johari [6], and Maxworthy [7] is simpler because a single vortex was treated in isolation. Additionally, these studies considered a carrier fluid that was laminar. Our situation is more complicated in that our goal is to examine a large population of vortex cores occurring naturally in turbulent flows. These myriad of vortices interact amongst themselves and affect their neighbors, warranting measurements for a general class of turbulent flows. The present work is intended to address these needs. Specifically, we report results for the radial variation of circulation, tangential velocity, and vorticity within the core of vortices present in the axial plane of a self-similar turbulent axisymmetric jet. We also present results for centrifugal force and energy associated with vortices of different sizes.

Experimental Setup and Eduction Technique

PIV measurements were conducted in a 1.2-m-tall glass tank with a 0.5-m-square cross section, which houses a nozzle at the bottom (orifice diameter, $d=2$ mm). Twin Nd-YAG pulsed lasers (350 mJ/pulse at 532 nm) provided illumination for PIV with a pulse separation of 12 ms. 8-μm hollow spherical glass particles were used as tracers for PIV with water as the working fluid. Recording was done using a Kodak 1.0 ES camera with a 1026 $\times$1000 pixels array. The view frame at $110 \leqslant z/d \leqslant 175$ was centered on the jet axis, with the edges of the frame extending to $\pm 1.5b$ (b is defined as the radial location at which the mean streamwise velocity reduces to e^{-1} of the mean centerline velocity). Measurements were conducted for jet Reynolds number, Re (based on d and the exit velocity) of 3000. See Agrawal and Prasad [2] for additional details.

The definition of Robinson et al. [8]—"A vortex exists when instantaneous streamlines mapped on to a plane normal to the core exhibit a roughly circular or spiral pattern, when viewed in a reference frame moving with the center of the vortex core," is used here for the definition of a vortex. Vortices were educed using the high-pass filtering technique (Adrian et al. [1], and Agrawal and Prasad [2]) in which the instantaneous field is first smoothed using a Gaussian kernel. Next, the resulting low-pass field (with the higher frequencies suppressed) is subtracted from the original velocity field, exposing the vortices which represent the high-frequency content in the velocity signal. The standard deviation of the Gaussian kernel was three grid units, and the filter was truncated at five grid units. These parameters were chosen carefully to expose all vortices. An illustration of the high-pass filtering operation on a small subset of the total PIV frame is provided in Fig. 2. It was verified that all the vortices in the high-pass field could also be identified by an alternate technique, viz. Galilean transformation, [1–3].

An automated method was employed to identify the vortices. A vortex center was located if the high-pass filtered velocity vectors displayed a monotonic variation in angular orientation from 0 to 2π while moving in a closed path around it. A point was accepted as a vortex center, r_0, if seven out of eight neighboring points satisfied the above criterion. The outermost radial position enclosed by a closed streamline determined the radius of the vortex, R. It should be noted that we are using the concept of "closed streamline" to mean that in the instantaneous, two-dimensional

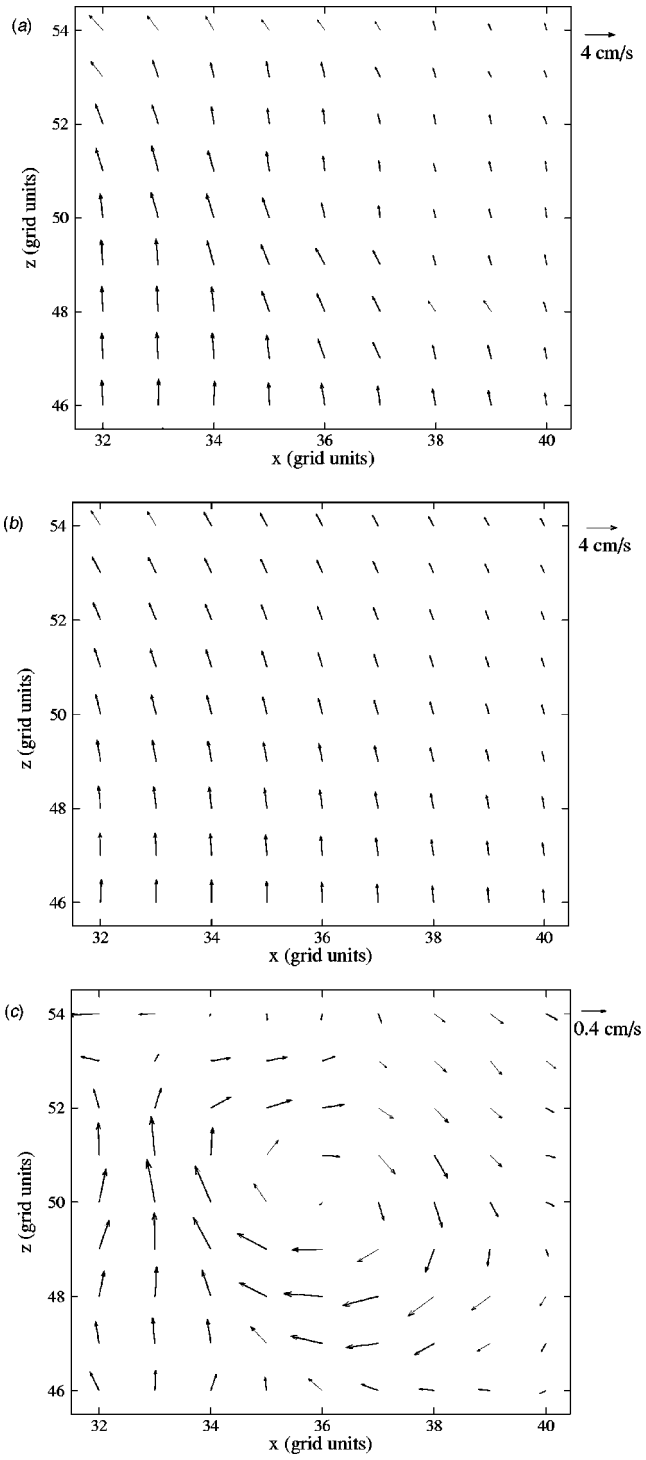

Fig. 2 (*a*) Instantaneous, (*b*) low-pass filtered, and (*c*) high-pass filtered vector fields (1 grid unit=2 mm)

PIV vector field, the integration of the velocity data will produce streamlines which are closed around the vortex center. In reality, because our flow field is turbulent (three-dimensional, dissipative, and unsteady (albeit stationary)) the streamlines that we identify for our eduction process need not coincide with the actual streamlines in the flow. Our usage of the term merely provides a simple way to identify a vortex center, and to measure the size of the vortex. An example of a high-pass filtered field with the identified vortices can be found in [2].

Agrawal and Prasad [2] employed an automated procedure with the above criteria to identify vortices with radii equal to *integer*

grid units. This procedure has been extended here to also identify vortices with non-integer radii and obtain improved resolution. The modified algorithm is thus able to resolve two new radii at $\sqrt{5}$ and $\sqrt{8}$ grid units between vortices of radii 2 and 3 grid units, and so on. Thus, we can now distinguish vortices of sizes 1, $\sqrt{2}$, 2, $\sqrt{5}$, $\sqrt{8}$, 3, $\sqrt{10}$, $\sqrt{13}$, and 4 grid units (note, each number is the square root of the sum of the squares of two integers), increasing the resolution from four to nine levels. The increased resolution provides sufficient datapoints to probe the vortex core with confidence. It was verified that the results from the current enhanced eduction program match that of [2], validating the robustness of the new method.

Vortex radius (R), rotational sense, and circulation (Γ) were measured directly here whereas tangential velocity (v_θ), vorticity (ω), centrifugal force (F_c), and energy (E) were derived. Circulation is calculated by integrating along a circular path centered at r_0:

$$\Gamma = \oint \mathbf{u}' \cdot d\mathbf{s},$$

where, $\mathbf{u}'$ denotes the high-pass filtered velocity field. The derived quantities are expressed as follows:

$$v_\theta(r) = \text{tangential velocity at } r = \frac{\Gamma(r)}{\pi r},$$

$$\omega(r) = \text{vorticity at } r = \frac{\Gamma(r)}{\pi r^2},$$

$$F_c(r) = \text{centrifugal force at } r = r\omega^2(r) = \frac{\Gamma^2(r)}{\pi^2 r^3},$$

where r is the distance from the vortex center, r_0. The energy of the vortex was obtained as

$$E = c_1 \Gamma^2(R),$$

where c_1 is a constant. (We set $c_1 = 1$ for the energy plots presented herein.)

Experimental Uncertainty. The rms value of any vortex property (such as circulation, tangential velocity, or vorticity) can be determined directly from the large population of vortices that we have educed for each value of R. As evident in Table 1, we have a sizable population of vortices from which we can draw reliable statistical results. We will focus on Γ in this section, because tangential velocity and vorticity are derived directly from Γ, therefore the relative uncertainty in their mean values would be the same as that of $\overline{\Gamma}$. Table 2 lists the normalized value of rms of circulation, $\sigma_\Gamma/\overline{\Gamma}$ for each value of R ranging from one to four grid units. Two sets of rms values are listed in Table 2, one corresponding to the center of the vortex (actually $r=1$) and the other corresponding to its edge ($r=R$). These rms values include the true variability in Γ, [2], as well as the errors accruing from the measurement process.

Table 1 Sample size for different vortex radii (based on a total of 10140 vortices from 222 PIV frames). (1 grid unit=2 mm.)

R (Grid Units)	Sample Size
1	3813
$\sqrt{2}$	2182
2	1253
$\sqrt{5}$	1204
$\sqrt{8}$	848
3	222
$\sqrt{10}$	58
$\sqrt{13}$	75
4	49

Table 2 Normalized rms, and the fractional uncertainty in the mean value of Γ for vortices of all R at the vortex center and vortex edge. Note that the uncertainties in v_θ and ω are identical to Γ as these quantities are derived from Γ. (1 grid unit = 2 mm.)

R (Grid Units)	At $r=1$		At $r=R$	
	$\sigma_\Gamma/\overline{\Gamma}$	$\Delta\overline{\Gamma}/\overline{\Gamma}$ (%)	$\sigma_\Gamma/\overline{\Gamma}$	$\Delta\overline{\Gamma}/\overline{\Gamma}$ (%)
1	0.60	1.9	0.60	1.9
$\sqrt{2}$	0.56	2.3	0.54	2.3
2	0.57	3.2	0.55	3.1
$\sqrt{5}$	0.48	2.7	0.42	2.4
$\sqrt{8}$	0.47	3.2	0.41	2.8
3	0.44	5.8	0.42	5.5
$\sqrt{10}$	0.39	10	0.33	8.5
$\sqrt{13}$	0.47	10.6	0.49	11.1
4	0.45	12.6	0.44	12.3

The rms values listed in Table 2 are sufficient to place uncertainty bounds (using the standard expression for 20 to 1 odds) on the mean quantities listed subsequently in this paper, such as $\overline{\Gamma}$, $\overline{v_\theta}$, $\overline{\omega}$. We will provide these results towards the end of this section. However, we will first show that the errors that arise from the measurement process amount to only a small fraction of the true variability in circulation.

The definition of Γ indicates that errors in measuring velocity and r will contribute to the error in Γ. For PIV measurements, the error associated with the measured velocity is determined primarily by the error in locating the correlation peak to subpixel accuracy. Our estimated value is about 1/10th of a pixel, which is a more or less standard value quoted by most PIV practitioners (Prasad [9]). The characteristic velocity scale in our flow (centerline velocity) corresponds to a displacement of about six pixels; consequently, the relative error in the characteristic velocity measurement is about 1.5%. In the current paper, we are interested in the high-pass filtered field which is obtained by subtracting the local mean velocity from the instantaneous velocity field. As seen by comparing Fig. 2(*a*) with Fig. 2(*c*), the characteristic velocity of the high-pass filtered field decreases by about one order of magnitude, therefore the *relative* error of the high-pass filtered field is amplified to about 15%.

The measurement of r is affected by the fact that the vortex center may not lie exactly on a grid point. In addition, not all closed streamlines are perfectly circular or even perfectly closed due to the nature of our eduction process and the criteria employed therein. Further, due to the discretizing nature of the eduction process, the true vortex radius may be slightly smaller or larger than the measured value. These effects can produce an additional random error in the value of Γ. It is not apparent that one can accurately quantify these errors without extensive modeling and simulations. However, we have roughly estimated that these sources will contribute an error of about 15% to 20%. Adding to this the uncertainty in velocity measurements, we obtain a cumulative (in a root-sum-square sense) measurement error in Γ of about 25%.

The rms values ($\sigma_\Gamma/\overline{\Gamma}$) listed in Table 2 can approach 40% to 60%. It is therefore apparent that the measurement error contributes only a small fraction to the total rms (note that the rms values must be combined in a root-sum-square sense). In fact, it is easily shown that the rms due to measurement error is only about 15% of the total rms. Most of the rms is therefore contributed by the genuine variability in Γ for a given R.

Finally, the uncertainty in the *average* value of Γ can be estimated using the standard expression (for 20 to 1 odds):

$$\Delta\overline{\Gamma} = \frac{1.96\sigma_\Gamma}{\sqrt{N}}$$

where N is the number of contributing vortices in the given ensemble. For example, from Table 1 $\sqrt{N}\approx 62$ for $R=1$ and 7 for $R=4$. Therefore, $\Delta\bar{\Gamma}/\bar{\Gamma}\approx 2\%$ for $R=1$ and 13% for $R=4$. $\Delta\bar{\Gamma}/\bar{\Gamma}$ values for vortices of all R are listed in Table 2 (at the center and at the edge).

Results and Discussion

Results presented in this paper pertain to a jet Reynolds number of 3000, with the view frame located between $110\leqslant z/d\leqslant 175$. Each PIV frame contains 60×60 vectors on a square grid (grid spacing$=2$ mm). Therefore the radius of the smallest resolved vortex is 2 mm, and the range of spatial scales that can be resolved here is about 30. The corresponding Kolmogorov length scale is approximately 0.2 mm, therefore the data is not fully resolved at the small scales. As noted in [2], the unresolved vortices will, however, not affect the results presented herein.

Results in this paper are based on a total of 10,140 vortices, corresponding to 222 PIV frames (average of about 46 vortices per frame). These vortices correspond to the self-similar regime of jets. Due to the turbulent nature of the flow, the distribution of vortices over space and time is somewhat random, implying that a different number of vortices will be captured in each frame. Figure 3 depicts the variations in the number of vortices in successive PIV frames. No noticeable trend is apparent, which confirms that the flow conditions are stationary.

A breakdown of the number total of vortices of different radii is shown in Table 1. The number of vortices present in the flow decreases monotonically with increasing R. Nevertheless, even for the largest vortices, the sample size is large enough to compute useful statistics. Figure 4 suggests that the number of vortices drops drastically beyond a certain size; therefore, two distinct curves are needed to fit the data. The expressions for the two curves are indicated in Fig. 4. Figure 4 helps to infer the presence of yet another regime for vortices smaller than 1 grid unit. Although these vortices are too small to be resolved from our current dataset, it should be obvious that the curve that fits vortices of size 1 to 2.8 grid units cannot be sustained indefinitely owing to a singularity as $R\rightarrow 0.5$. Eventually, viscosity will begin to dominate as the Kolmogorov scale is approached and a different curve fit will apply there. More detailed measurements at the smallest scales are required to confirm this extrapolation.

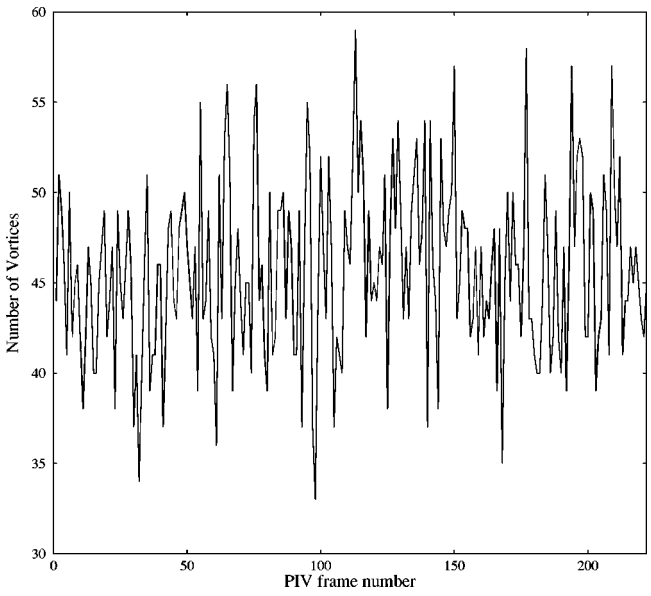

Fig. 3 Variation in the number of vortices in successive PIV frames for a typical run

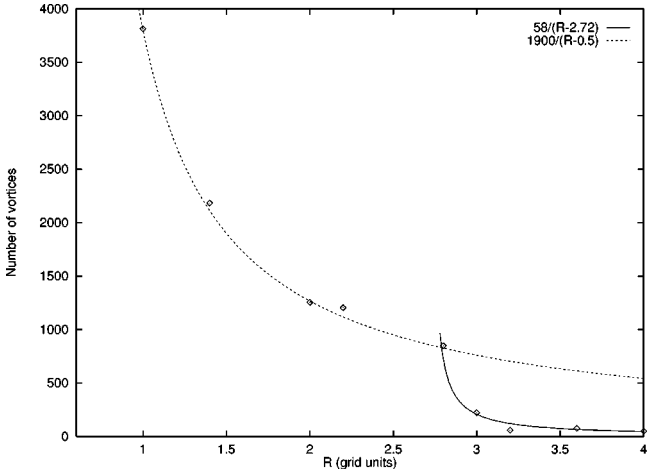

Fig. 4 Curve fits to number of vortices of different sizes (1 grid unit=2 mm)

Vorticity obtained by differentiating the instantaneous velocity map is qualitatively similar to that obtained by differentiating the high-pass filtered field (Figs. 5(*a*) and 5(*b*), respectively) indicating that the high-pass filtered field accurately represents the instantaneous vorticity field. The quantitative difference between Figs. 5(*a*) and 5(*b*) is because Fig. 5(*a*) represents the *total* vorticity, whereas Fig. 5(*b*) represents only the high-pass filtered vorticity. While Fig. 5 validates our education technique, the use of high-pass filtering in the first place warrants justification. The reason for employing the filtering technique is that our vortex identification and measurement scheme described above specifically looks for closed streamlines which are only seen in the high-pass filtered field.

Does the Largest Closed Streamline Represent the Core Size? As mentioned above, we denote the radius of the largest closed streamline as the vortex radius, making it important to understand the relation between them. A single vortex in a quiescent environment will present closed streamlines for all r. However, in a turbulent field, the presence of additional vortices with random circulations in the neighborhood will disturb the closed streamline pattern around any vortex. It can be expected that a given vortex will feel the presence of its neighbors more strongly beyond its edge corresponding to regions of small ω, whereas regions of high ω corresponding to the vortex core are less likely to be affected. Based on this qualitative argument, it is plausible that the region of high-vorticity concentration bounded by the largest closed streamline ($r<R$) would correspond to the vortex core.

The above conjecture was tested with a simulation using Rankine vortices. 44 Rankine vortices were placed on a 60×60 grid such that their number, center locations, rotational sense, and circulations corresponded to the vortices in a real (randomly chosen) PIV frame. Each Rankine vortex core size was assigned as R, the radius of the largest corresponding closed streamline. Therefore, $v_\theta\sim r$ for $r\leqslant R$, and as $1/r$ for $r>R$. While streamlines for an individual Rankine vortex are closed for all r, this is no longer true after superposing the velocity fields from all 44 vortices. This superposed velocity field was high-pass filtered and input into our vortex education program. It was found that for 50% of the resulting vortices, the vortex core size corresponded *exactly* to R. For the remaining vortices the largest closed streamline was *larger* than their prescribed cores (more so for isolated vortices compared to vortices occurring in close proximity). In no case did we find streamlines closing inside the prescribed core. This simulation supports our belief that the largest closed streamline encompasses the vortex core in its entirety.

The criterion of using the largest closed streamline to determine the vortex core size is also consistent from the point of view of

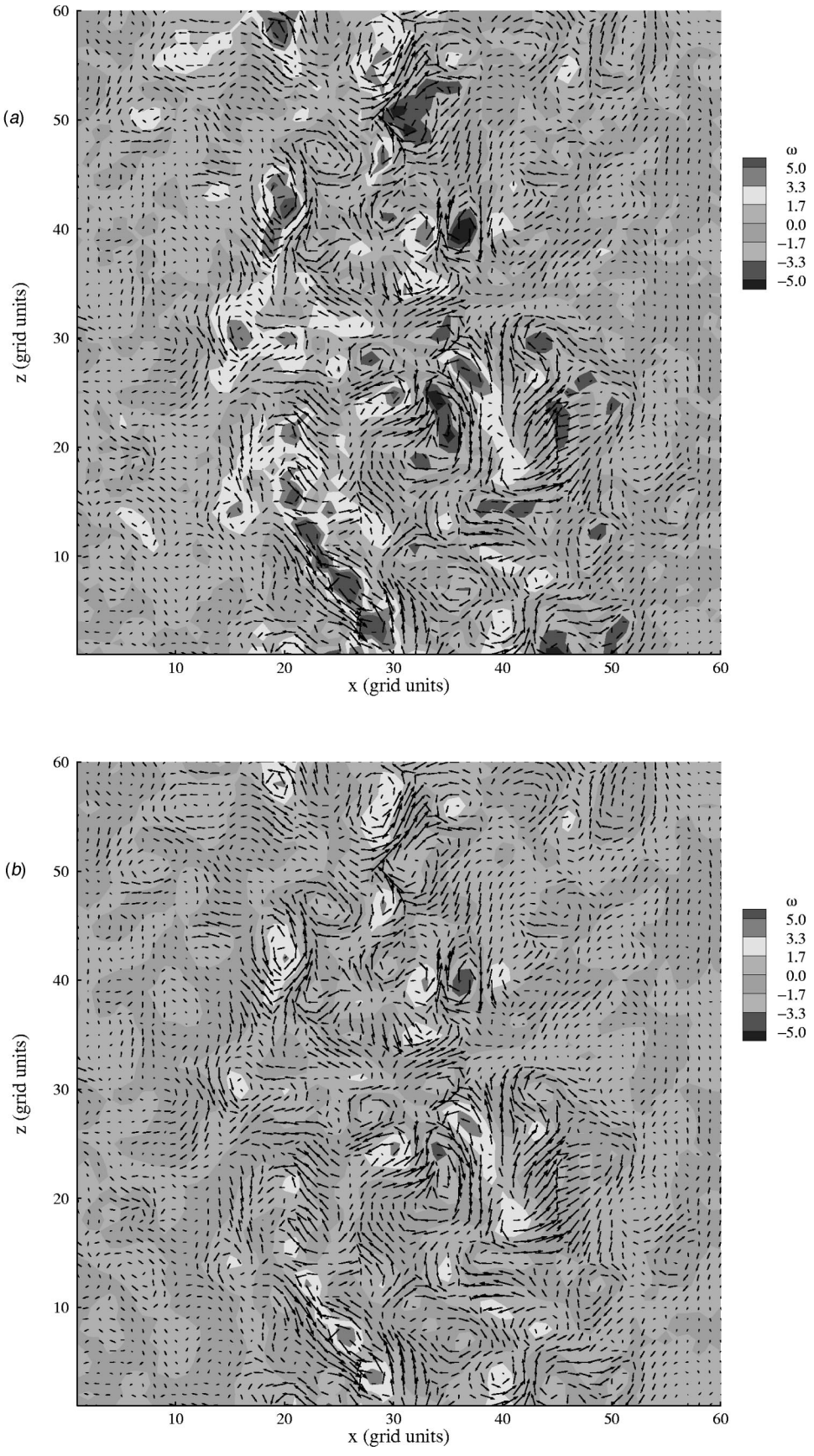

Fig. 5 Vorticity obtained by differentiating (*a*) instantaneous and (*b*) high-pass filtered field with overlaid high-pass field vectors

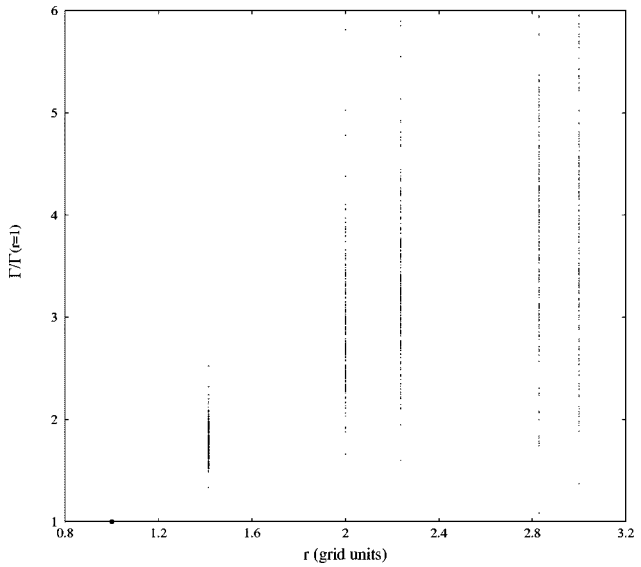

Fig. 6 Normalized circulation within vortices of radii $R=3$ grid units (total 222 vortices)

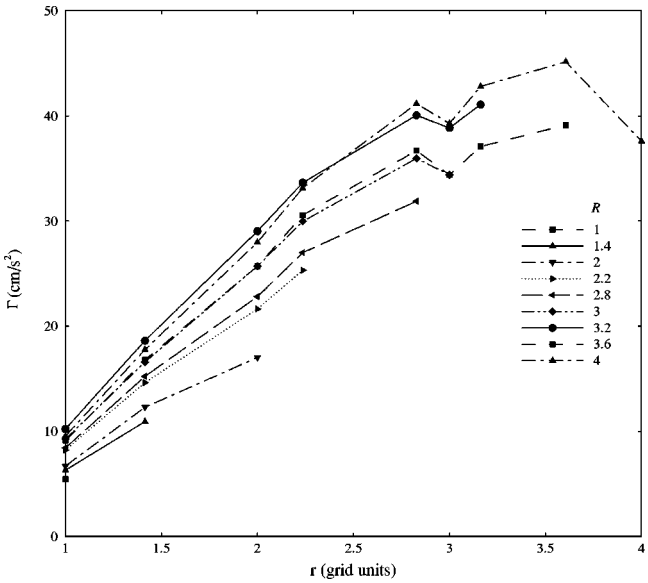

Fig. 7 Variation of average circulation within vortex cores for vortices of varying radii (1 grid unit=2 mm). See Table 2 for the values of the relative uncertainty in Γ.

circulation. For a Rankine vortex, Γ increases as r^2 within the core, and reaches a constant path-independent value once the entire core is encompassed within the path. Agrawal and Prasad [2] have demonstrated that for vortices in a turbulent jet flow, circulation does increase with r within the region of closed streamlines, and may increase or decrease beyond it depending for example on the presence and circulation of vortices in the neighborhood. This again indicates that the entire region where vorticity is present (the vortex core) is encompassed by the largest closed streamline, while no useful information about circulation or other properties can be extracted outside it.

Variation Within Vortex Cores

Circulation and Tangential Velocity. The radial variation of circulation within vortex cores is plotted in Fig. 6. For illustration purposes we chose circulation and $R=3$ grid units; however similar observations can be made for other properties and within vortex cores of other radii. For an easier comparison between vortices of different circulations, the results are normalized by the circulation at $r=1$. The scatter in the figure must be viewed in light of the fact that Fig. 6 includes data from 222 vortices (see Table 1), i.e., 222 data points exist for each r. The scatter in the circulation data is consistent with our expectation (see the earlier section on experimental uncertainty) that even vortices of a given size can exhibit a wide range in properties. The scatter increases monotonically with r, for example, the normalized rms is 0.19 and 0.39, respectively for $r=2$ and 3. However, the increase is scatter with r is simply an artifact of the normalization with respect to $\Gamma(r=1)$. As listed in Table 2, the value of $\sigma_\Gamma/\overline{\Gamma}$ is about 0.4 for all $r\leqslant 3$.

Figure 7 reveals that the ensemble averaged circulation increases with r inside the core, and tends to plateau near the core edge. As noted earlier, circulation is expected to display such a behavior within vortex cores. Moreover, for a given r, larger vortices have larger Γ associated with them.

Figure 8 shows polynomial fits to the ensemble averaged data for circulation for vortices of $R=3$ grid units. Figure 8 reveals that for real vortices, $\Gamma\sim r^2$ is valid only for a very small subregion inside the vortex core ($r<1.4$). $\Gamma\sim r$ for $1.4\leqslant r\leqslant 2.4$. Finally for $r>2.4$, Γ is seen to vary as $r^{0.8}$. The different polynomial fits to the data reveal that a real $R=3$ vortex is similar to a Rankine vortex only for $r<1.4$, and differs substantially from it beyond $r=1.4$. In fact, the latter fits help to identify possible alternate regimes (for example, constant v_θ region, see below), and to characterize the deviation of a real vortex from a Rankine vortex.

Figure 9 shows that the radial variation of ensemble averaged v_θ is nonmonotonic in nature. For most R it is seen to increase and then decrease, with maximum v_θ lying within the vortex core. Based on the fit in Fig. 8, it can be concluded that on an average v_θ varies almost linearly deep inside the core, remains constant for a large part, and then decreases as $r^{-0.2}$ towards the edge. The somewhat linear increase in v_θ indicates that the flow very close to the vortex center undergoes a solid-body-like rotation. It should be noted that while this subregion of solid-body-like rotation is a small part of the entire vortex core, it assures that the dissipation remains bounded.

Vorticity. Figure 10 shows the ensemble averaged vorticity for various vortex sizes. Describing ω as a constant within the vortex core is clearly not apt, indicating that the approximation to a

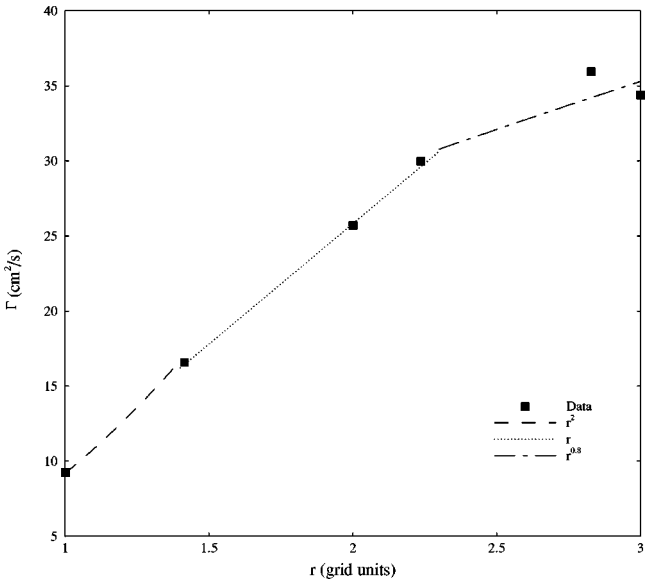

Fig. 8 Polynomial fits to average circulation for vortex radius =three grid units

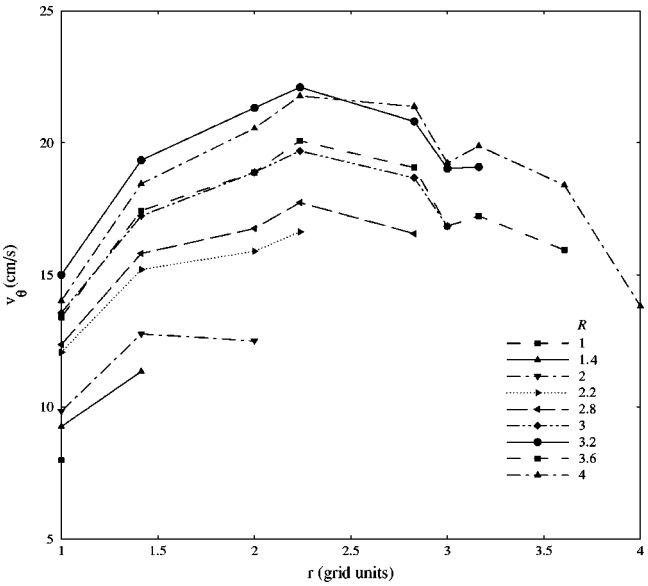

Fig. 9 Variation of average tangential velocity within vortex cores for vortices of varying radii. See Table 2 for the values of the relative uncertainty in v_θ.

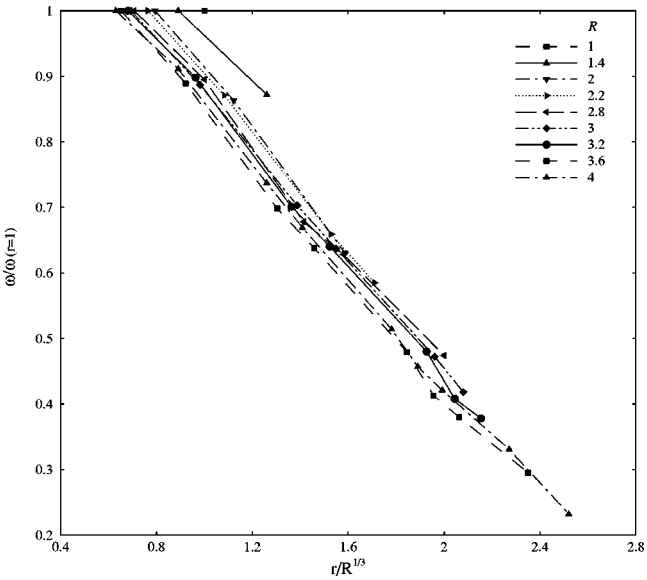

Fig. 11 Normalized vorticity within vortices of different radii

Rankine vortex is not perfect. The maximum value of ω occurs at $r=1$, and decreases monotonically with r. The plot (Fig. 10) looks qualitatively similar to Fig. 1. Thus we have verified experimentally the trend depicted in Kundu's [4] schematic drawing (Fig. 1).

Another interesting observation can be gleaned from the plot by carefully following the vorticity values from different vortex radii. It is commonly assumed that most of the vorticity in turbulent flow is associated with small scales which is consistent with the belief that on average a large vortex will overturn slower compared to a small vortex. However, Fig. 10 reveals that at least for the range of vortices investigated herein this is *not* necessarily true. Compared to their smaller counterparts large vortices exhibit a larger ω at the center. The list of vortices with highest to lowest vorticity at the core reads as $R=3.2$, 4, 3, 3.6, 2.8, 2.2, 2, 1.4, 1. Although two (out of a total of nine) vortices occur out of sequence, the general trend is from the largest to the smallest R, and the outliers may be attributed to experimental jitter resulting from a combination of measurement error and the true variability in ω. As stated in the earlier section on experimental uncertainty, the uncertainty in mean vorticity can approach about 13% in the worst case. This uncertainty could account for the nonmonotonic behavior of the list.

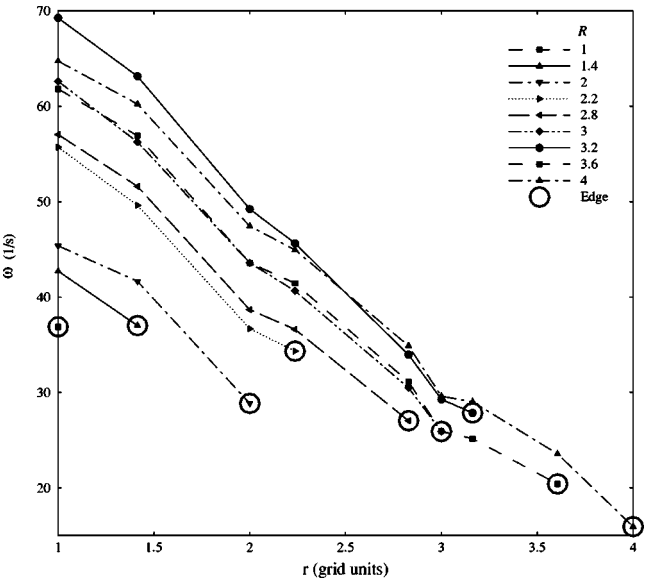

Fig. 10 Variation of average vorticity within vortex cores for vortices of varying radii. See Table 2 for the values of the relative uncertainty in ω.

As one progresses towards the edges of these larger vortices, ω drops to a value smaller than the corresponding value at the core-edge of smaller vortices, i.e., the terminal value of ω decreases as R increases. This is highlighted in Fig. 10 by the use of a special symbol (heavy circles). The list of vortices with highest to lowest vorticity at the edge reads as $R=1.4$, 1, 2.2, 2, 3.2, 2.8, 3, 3.6, 4. Although the variation is not perfectly monotonic (three outliers out of a total of nine) a downward trend in ω with increasing R is quite apparent. Figure 10 supports the contention that the classical picture only applies at the core edge, and *not* throughout the core of the vortex. Again, experimental uncertainty could account for the outliers in the list.

Additional insights about vortices can be obtained if a suitable scaling is available by which data can be collapsed. This motivated us to find appropriate ways to normalize the results. Dimensionally homogeneous relationships were sought initially, but these did not lead to a successful collapse of the data. Instead, it was found that a dimensionally inhomogeneous expression of the form

$$\frac{\omega}{\omega_c}=f\left(\frac{Br}{R^n}\right),$$

showed promise. Here ω_c denotes the value of vorticity at the vortex center; however, because of our inability to measure it we used $\omega(r=1)$, and B denotes a constant. $n=1/3$ gave the most satisfactory collapse of the vorticity values from different vortex-radii (see Fig. 11). While the lack of dimensional homogeneity is somewhat unsatisfactory, it should be noted that the collapse is not dependent on the units that are used for the length scales as the differences can be absorbed in the constant B. Results are particularly good for $R\geqslant 2$. Vortices with $R\leqslant\sqrt{2}$ lying above the normalized curve are explained as follows.

$\omega(r=1)$ underestimates the vorticity at the center, with the difference between ω_c and $\omega(r=1)$ increasing with decreasing R. The difference becomes substantial for small vortices ($R\leqslant\sqrt{2}$). Therefore, the vorticity value does not fall on the normalized curve, rather it falls above it. A direct advantage of normalization is that the correct value of ω_c can be estimated from the normal-

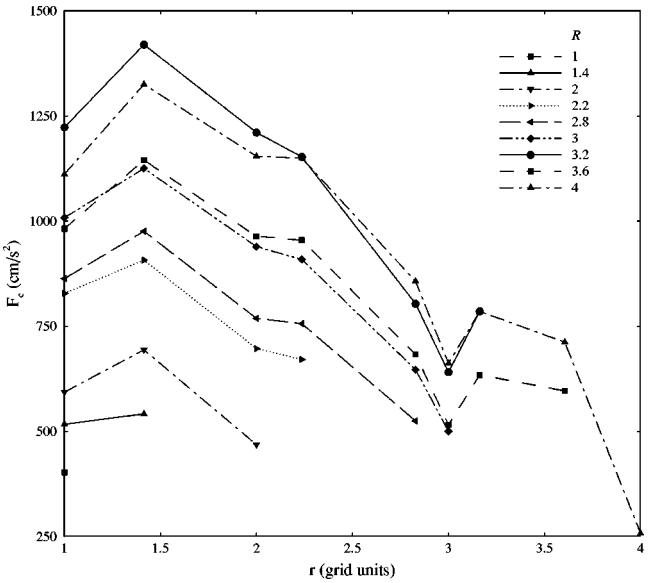

Fig. 12 Variation of average centrifugal force within vortex cores for vortices of varying radii

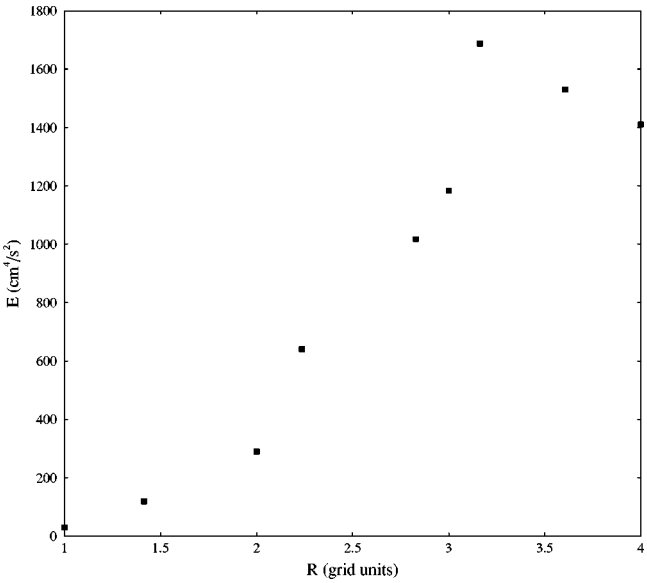

Fig. 13 Average energy associated with different vortex radii

ized curve. This is all the more useful for vortices of smaller radii. For example ω_c for $R=1$ is estimated as $53s^{-1}$ corresponding to a difference of about 30% from $\omega(r=1)$.

Centrifugal Force and Energy. Knowledge of the centrifugal force, F_c within vortex cores is important because like other body forces it can induce relaminarization. From a purely practical viewpoint, radial variation of F_c is relevant in planning PIV measurements. If the density of the fluid and seeding particles are mismatched, particles may not track the flow well. Regions of large vorticity are particularly susceptible to errors. It is expected that particles (with density greater than the fluid) will be centrifuged out of the vortex core, resulting in a poor particle concentration near the vortex center and an increased concentration near the core edge (our measurements are not affected by this because the density of particles was matched to that of the carrier fluid). This makes it important to know the radial variation of F_c within the vortex core.

For a Rankine vortex, F_c increases linearly in the core, and decreases as $1/r^3$ beyond it. Therefore, F_c can be expected to be a maximum at the core edge. The plot for a real vortex core is, however, nonmonotonic (Fig. 12), increasing slightly followed by a monotonic decrease. The increase corresponds to the solid-body-like rotation subregion (constant ω but increasing r). The subsequent decrease is consistent with the fact that ω decays faster than $r^{-1/2}$. Interestingly, the plot reveals that the maximum centrifugal force occurs between the vortex center and the edge (and not at the core edge).

Energy of the vortices for different radii is depicted in Fig. 13. It can be seen that the average energy associated with a given vortex radius increases as R^2 for the range of vortex sizes investigated. Therefore, the qualitative nature of the curve for energy versus vortex radius is in accordance with the classical theory of turbulence, i.e., average energy of vortices should increase with their size.

Conclusions

Measurements inside vortex cores have provided new insights into the nature of vortices in a turbulent field. The criterion of closed streamlines was used to identify vortices in a turbulent jet, and methods were developed to measure the properties within the vortex core. It is argued here that for turbulent flows with a myriad of underlying vortices, the largest closed streamline bounds the vortex core. Three possible regimes of vortex number versus vortex size are suggested by our data. The vortex-core has a small solid-body rotation like subregion (constant vorticity). However for a large part of the vortex core, the tangential velocity remains a constant. Subsequently near the core edge the tangential velocity decreases as $r^{-0.2}$.

There is substantial evidence to support that the centers of smaller vortices rotate slower than those of large vortices (although the variation is not perfect due to experimental uncertainty); however, the trend reverses near the core edge. Therefore, it can be concluded that the classical picture is only applicable for the core edge, and *not* throughout the core of the vortex and that the general understanding of turbulence implicitly refers to the vorticity at the core edge. An expression to normalize the vorticity from different vortex radii can be utilized to estimate the correct value of vorticity at the vortex-center for smaller vortices. In accordance with the turbulence theory, the average energy of the vortices is seen to increase with the vortex radius. In fact, the average energy appears to increase as the square of the vortex radius for the range of vortex sizes investigated here.

Acknowledgments

This work was supported by National Science Foundation, under grant NSF-ATM-9714810.

References

[1] Adrian, R. J., Christensen, K. T., and Liu, Z.-C., 2000, "Analysis and Interpretation of Instantaneous Turbulent Velocity Fields," Exp. Fluids, **29**, pp. 275–290.
[2] Agrawal, A., and Prasad, A. K., 2002, "Properties of Vortices in the Self-Similar Turbulent Jet," Exp. Fluids, **33**, pp. 565–577.
[3] Agrawal, A., and Prasad, A. K., 2003, "Organizational Modes of Large-Scale Vortices in an Axisymmetric Turbulent Jet," Flow, Turbul. Combust., **68**, pp. 359–377.
[4] Kundu, P., 1990, *Fluid Mechanics*, Academic Press, San Diego, CA.
[5] Mayer, E. W., and Powell, K. G., 1992, "Similarity Solutions of Viscous Vortex Cores," J. Fluid Mech., **238**, pp. 487–507.
[6] Desabrais, K. J., and Johari, H., 2000, "Direct Circulation Measurement of a Tip Vortex," AIAA J., **38**, pp. 2189–2191.
[7] Maxworthy, T., 1977, "Some Experimental Studies of Vortex Rings," J. Fluid Mech., **81**, pp. 465–495.
[8] Robinson, S. K., Kline, S. J., and Spalart, P. R., 1989, "Quasi-Coherent Structures in the Turbulent Boundary Layer. Part II: Verification and New Information From a Numerically Simulated Flat-Plate Boundary Layer," *Near Wall Turbulence. Proceedings of Zaric Memorial Conference*, edited by S. J. Kline and N. H. Afgan, eds., Hemisphere, New York, pp. 218–247.
[9] Prasad, A. K., 2000, "Particle Image Velocimetry," Curr. Sci., **79**, pp. 101–110.